nominal value leads to nonuniformities of the coolant flow rate along the channel of the order of 40%. Estimate of the value of the parameter of heat transfer between disk coils for T-15 gives $K_\perp = 80$. It is evident from Fig. 4 that the point corresponding to these values lies above the curve $t_e = 0.2$, so that the disk coils of the superconducting winding cool down at practically the same rate.

NOTATION

c, specific heat capacity, J/(kg•K); G, mass flow rate of the coolant, kg/sec; g, magnitude of the nonuniformity of the distribution of the coolant flow rate in a system of two channels; H and h, width and thickness of the conductor, m; I, number of disk coils in the winding; i, number of the disk coil; $K_\perp$, $K_\parallel$, dimensionless thermal interaction parameter between neighboring disk coils and between neighboring loops of the spiral; L, length of the cooling channel, m; M, mass, kg; m, mass per unit length of the channel, kg/m; N, number of loops in the spiral; Q, dimensionless thermal load per unit length; $R_\parallel = \delta/(\lambda H)$, $R_\perp = \delta/(\lambda h)$, thermal resistance of a unit length of the insulation layer between neighboring loops of the disk coil and between disk coils, K•m/W; T, temperature, °K; t, dimensionless time; X and x, dimensionless and dimensional (m) spatial coordinates; δ, thickness of the interloop insulation, m; λ, coefficient of thermal conductivity of the insulation, W/(m•K); $\Theta = (T_w - T_{fin})/(T_{ini} - T_{fin})$, dimensionless excess temperature of the wall; $\Delta\Theta$, dimensionless temperature difference; τ, time, sec; $\tau_b = (Mc)_\Sigma/(Gc_p)_\Sigma$, heat-balance cooldown time, sec; $St^* = \alpha\Pi L/(Gc_p)_g$, modified Stanton parameter. The indices are: p, constant pressure; w, wall; ini, fin, initial and final states; Σ, total value; e, equalization time of the temperature; max, maximum value; and g, gas.

LITERATURE CITED

1. S. P. Gorbachev, A. A. Krikunov, and V. A. Sysoev, Processes, Technology, and Control in Cryogenic Machine Building [in Russian], Balashikha (1979), pp. 20-29.
2. S. P. Gorbachev, A. A. Krikunov, and S. D. Ladokhin, Reports at the 2nd All-Union Conference on Engineering Problems for Thermonuclear Reactors, Vol. 2 (1982), pp. 152-158.
3. B. A. Vakhnenko and A. V. Filippov, Thermophysical Problems in Nuclear Power Plants [in Russian], Moscow (1986), pp. 106-112.

INTERNAL STRUCTURE OF COMPOSITE MATERIALS BY USING COMPUTER TOMOGRAPHY

V. I. Barakhov, I. P. Dimitrienko, V. I. Goncharov, A. P. Stepanov, and V. A. Nikolaev

UDC 541.18+539.217.1

Results are presented of tomographic investigations of the internal structure parameters of composite materials characterized by an elementary cell density distribution over the specimen volume.

To solve many characteristic heat and mass transfer problems in shells of composite materials, a preliminary investigation of properties of their internal structure is necessary. The quantity of inhomogeneities and defects, their size, orientation, and mutual location in space will predetermine elapsing processes to a great extent. The predominance of any transfer mechanism and the very physics of the phenomenon depend on the internal structure of composites.

Utilization of x ray computer tomography affords great possibilities in investigations. Without disturbing the integrity of the shell specimen it permits reconstruction of the pattern of its spatial sections, measurement of the geometric dimensions and the relative arrangement of internal structure elements, and a quantitative estimation of the density distribution of the material and the porosity in any section of the specimen.

Translated from Inzhenerno-Fizicheskii Zhurnal, Vol. 51, No. 6, pp. 1021-1027, December, 1986. Original article submitted October 29, 1985.

0022-6841/86/5106-1476$12.50

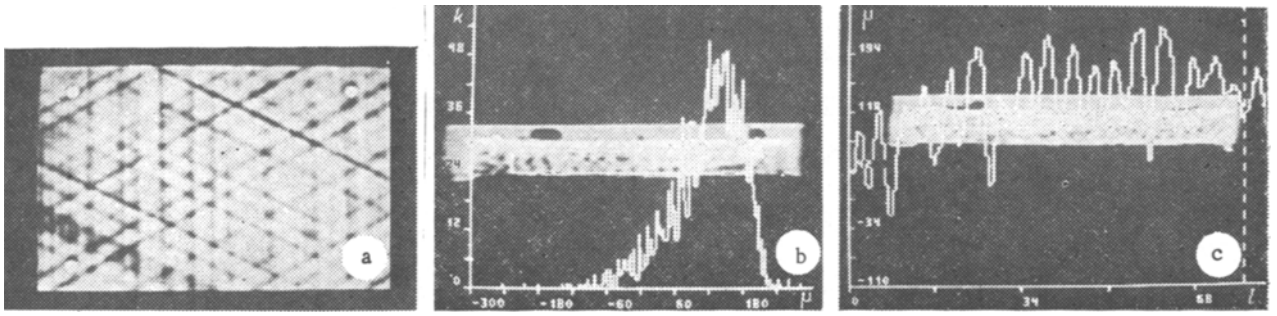

Fig. 1. Reconstruction of the specimen longitudinal (a) and transverse (b, c) sections. $l \cdot 10^{-3}$, m.

The method is based on scanning and measuring the photon intensity of x radiation after passage through the substance of the object. The intensity of the radiation being recorded will here depend on both the radiation energy and the structural inhomogeneities of the substance of the object in the path of the beam. After the measurement results have been processed mathematically, we obtain a matrix of numbers that characterize the radiation absorption and scattering by each elementary cell of the specimen section being investigated. Quantitatively, this capability is characterized by the linear attenuation factors (LAF), the Houndsfield numbers. The LAF is an integral characteristic for each elementary cell (parallelepiped).

At the present time a number of rigorous mathematical methods have been developed that permit the accurate reconstruction of a two-dimensional LAF distribution $\mu(x, y)$ from a discrete system of accurate measuring data on radiation attenuation by the specimen under investigation [1, 2]. The combined influence of scattering and absorption results in exponential damping of the photon beam as it passes through the specimen material:

$$I = I_0 \exp\left[-\int_A^B \mu(x,\ y)\, dy\right]. \tag{1}$$

Utilization of one plane for multiple radiation permits reduction of the dimensionality of the problem, which reduces to restoration of the two-dimensional distribution $\mu(x, y)$ from known one-dimensional projections. We obtain from (1) for the normalized magnitude of the linear projection

$$P(r,\ \varphi) = \ln \frac{I_0(r,\ \varphi)}{I(r,\ \varphi)} = \int_{r\varphi} \mu(x,\ y)\, ds, \tag{2}$$

where

$$r = x\cos\varphi + y\sin\varphi. \tag{3}$$

Therefore, the problem of reconstructing the image in computer tomography reduces to solving the integral Eq. (2) while finding $\mu(x, y)$ from measured values of $P(r, \varphi)$.

The internal structure of a polymer composite was investigated on the computer tomograph SOMATOM DR2. The image was reconstructed here on the basis of a reverse projection method with filtration on the basis of convolution. Taking account of (2) and (3), the reverse projection procedure can be written in integral form as

$$\mu(x,\ y) = \int_0^{\pi} P(x\cos\varphi + y\sin\varphi,\ \varphi)\, d\varphi, \tag{4}$$

where

$$P(r,\ \varphi) = \int_{-\infty}^{\infty} P(k\varphi)\exp(2\pi jkr)\, dk. \tag{5}$$

We can then obtain

$$\hat{\mu}(x,\ y) = \int_0^{\pi}\int_{-\infty}^{\infty} \frac{P(k\varphi)}{|k|}\exp\left[2\pi jk\left(x\cos\varphi + y\sin\varphi\right)|k|\right] dk\, d\varphi. \tag{6}$$

Evaluating (6) after detector measurements of $P(r, \varphi)$ in the form of the convolution of two functions by using an approximation by one-dimensional finite sums on an electronic computer, we will have a matrix of LAF values after filtration.

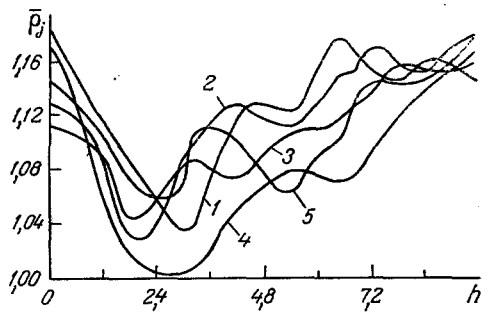

Fig. 2

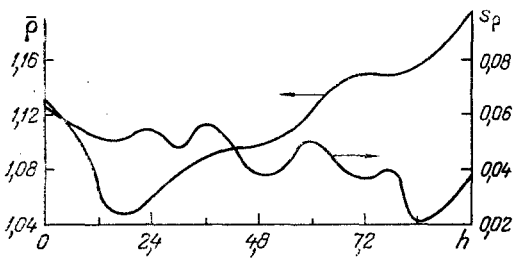

Fig. 3

Fig. 2. Curves of the change in density $\bar{\rho}_j \cdot 10^{-3}$ (kg/m^3) over the specimen thickness for its different sections. Numbers at the curves are the specimen sections.

Fig. 3. Curves of the change in the mathematical expectation $\bar{\rho} \cdot 10^{-3}$ and the root mean-square deviation $s_\rho \cdot 10^{-3}$ (kg/m^3) over the specimen thickness.

For organic plastics the correspondence between the true density ρ and the LAF $\mu(x, y)$ can be expressed approximately in the form of the following formula:

$$\rho = 1 + 97{,}75 \cdot 10^{-5} \mu. \tag{7}$$

Therefore, by converting the matrix $M(\mu_{ij})$ into the matrix $P(\rho_{ij})$, the value of the density of each elementary cell of theinternal structure of the specimen can be obtained. Its dimensions are characterized by the scanning layer thickness d and the zoom factor z.

Organic plastic specimens $(60 \times 90 \times 10) \cdot 10^{-3}$ m cut out of a pre-loaded cylindrical shell were investigated. They passed through dryer before the tomography. Scanning was performed on a tomograph for $d = 8 \cdot 10^{-3}$ m. Image reconstruction was realized on an electronic computer with the zoom factor $z = 4$. A qualitative analysis of the internal structure can be executed on the reconstruction of the image reconstruction reproducible on the screen of a half-tone display where the shadow image with a definite grey level gradation is set in correspondence with the Houndsfield numbers. The stratifications formed in the winding of the spiral and tangential layers of the shell, the voids, and the zones of reduced density in the transverse section of the specimen are seen clearly in the photographs (Fig. 1a) of the longitudinal and transverse (Fig. 1b, c) sections of one of the specimens investigated. The LAF values of such zones on the matrix list are a group of numbers with the sign (—). A characteristic section of the matrix for one of the specimens investigated is presented below:

116	120	102	89	83	98	109	112	118	111
166	122	55	—7	—48	—1	68	116	129	129
173	138	53	—29	—73	—45	35	92	120	118
126	89	44	16	7	26	58	73	77	71
61	21	14	43	92	120	124	93	54	31
13	—30	—33	8	51	82	83	63	28	0
14	3	13	16	28	32	23	16	—11	—22
32	68	96	111	101	98	95	69	38	38

For air the LAF value is $\mu = -1023$ while $\mu = 0$ for water. If the LAF values for an elementary cell lie between the limits $0 \geq \mu \geq -1023$, then a large air-filled pore is in its volume.

We use the following functional dependences to investigate the properties of the internal structure of a material:

the mathematical expectation of the density over the thickness (h) of the specimen $\rho = f(h)$;

the root-mean-square deviation over the specimen thickness $s_\rho = f(h)$;

the density distributions for fixed sections corresponding to h_i $(i = 1, 2, \ldots, m) f_i(\rho)$;

the density over the specimen length for the section being recorded $\rho_i = f(l)$.

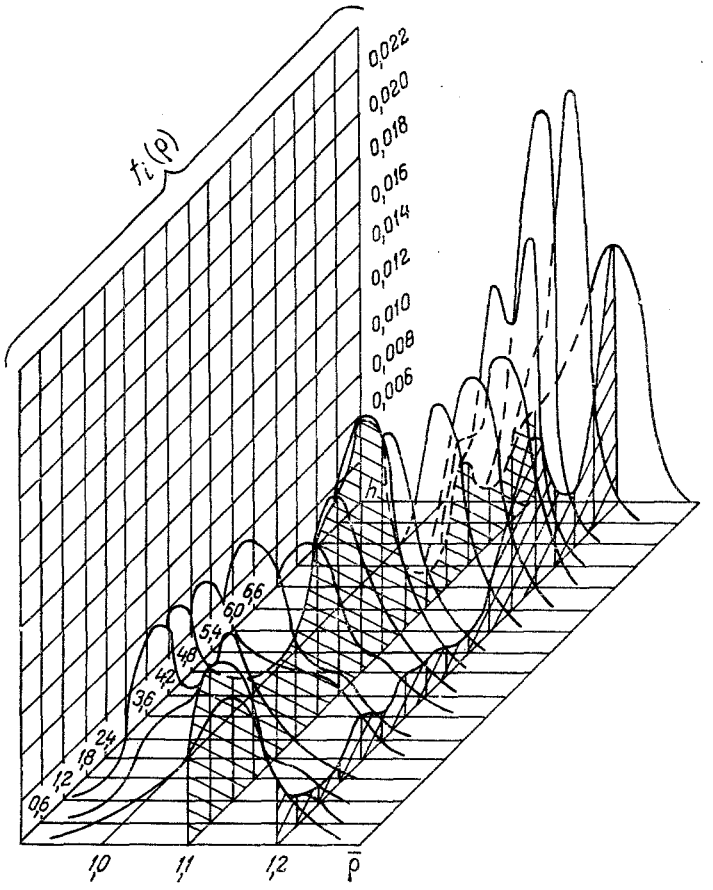

Fig. 4. Empirical density distribution functions. $h \cdot 10^{-3}$, m; $\rho \cdot 10^{-3}$, kg/m^3.

In order to compare the densities of the internal structures of different sections of the material we divide the specimen section under investigation into five identical adjacent rectangular elements, each of which is characterized by a matrix of density values for the elementary cells P (17 × 20). As is seen from Fig. 2, the density of the internal structure of separate elements of a composite specimen is heterogeneous. The curves of the mathematical expectation of the density over the thickness are oscillatory in nature with a common tendency to a reduction in the values as the shell external surface is approached. The rise in the density curves at the external surface is due to the winding conditions: the last layers were wound with an elevated binder content. Such a nature of curve behavior for the material being investigated is generally illogical. Because the percentage of binder is here greater and it is of an approximately 1.2 times lighter fiber, a further reduction in the density should occur in the external layers, while the reverse is observed in the graphs of $\bar{\rho}_j = f(h)$ (Fig. 2). This is explained by the reduction in porosity in layers with a high percentage of binder.

A graph of the function $\bar{\rho} = f(h)$ computed for the whole matrix of LAF values is presented in Fig. 3. By comparing the shell winding diagram with the curve $\bar{\rho} = f(h)$ it can be noted that the inflection points of the curve correspond to sites of a change in tension during passage from spiral to tangential layers, and vice-versa. To solve heat and mass transfer problems it is necessary to know the analytic expression for the dependence $\bar{\rho} = f(h)$. The experimental curve represented in Fig. 3 can be approximated by a polynomial of tenth degree

$$\bar{\rho} = 1{,}202 + 1{,}036 \cdot 10^{-2} h - 1{,}912 \cdot 10^{-3} h^2 - 1{,}149 \cdot 10^{-1} h^3 + \\ + 1{,}272 \cdot 10^{-1} h^4 - 6{,}024 \cdot 10^{-2} h^5 + 1{,}553 \cdot 10^{-2} h^6 - \\ - 2{,}343 \cdot 10^{-3} h^7 + 2{,}065 \cdot 10^{-4} h^8 - 9{,}863 \cdot 10^{-6} h^9 + 1{,}973\, h^{10}.$$

The approximation error in this case is calculated from the formula

$$C = \frac{\sum_{i=1}^{L} (\rho_{i_t} - \rho_{i_e})}{L - n}. \quad (8)$$

For n = 10, C = C_{min} = 0.0045. The coefficients of the polynomial were determined by the "MATEK" program compiled in the language PL-1. The program is based on using least squares and permits selection of the degree of the polynomial describing the experimental curve by using minimization of the approximation error.

The degree of structure heterogeneity along the specimen thickness can be estimated from the curve $s_\rho = f(h)$ (Fig. 3). Analysis of this curve shows a general tendency to an increase in the scattering of the density values as the specimen external surface is approached, which is explained by an increase in the heterogeneity of the external structure because of the appearance and broadening of the reduced density zones.

The matrix of elementary cell density values affords a possibility for constructing empirical distribution functions $f_i(\rho)$ for each i-th section over the specimen thickness. They are determined by processing the statistics in the i-th row of the matrix. Empirical distribution curves for 17 internal structure sections are obtained for one of the specimens under investigation in conformity with the image reconstruction for z = 4 (Fig. 4) because of processing tomography data according to the program "STATIK" on an electronic computer.

To analyze the results obtained, it is necessary to determine the factors affecting the distribution of the density values at the boundaries of its dispersion. In this case three dominant factors can be separated out: 1) the presence of a bonding filler in the material; 2) its fabrication by using a polymer host; 3) the presence of pores, cracks, voids.

The spread of the parameters characterizing each of these factors forms a field of possible density values of the specimen internal structure. Taking into account the relationship between the density values of the filler and the binder, it can be assumed that the nature of the right branch of the distribution functions obtained is predeetermined by the bonding braid parameters, and the left by the binder and pore parameters. Analyzing the distribution curves obtained as well as the curves that are reproducible after tomographic processing of the scanning data in the zone of interest on a halftone display screen (see Fig. 1b), it can be concluded that distribution curves with negative asymmetry are dominant. Therefore, the bonding filler in a material in a state of tension has a considerably smaller field of possible density values as compared with the binder. This same relationship is also conserved for individual investigations of material components.

Certain sections of the specimen under investigation have significant reduced density domains. The distribution functions in these sections are unimodal (Fig. 4). The factor of the presence of pores becomes so significant here that it results in the appearance of a second peak in the distribution function.

The tomographic method of investigating the internal structure of composite material specimens permits the construction of the density change on a line along a selected direction on a half-tone display screen after the image has been reconstructed. By using metal stubs inserted into the material as coordinates for the selection of the interesting direction, a graph of the density change can be constructed as a function of the specimen length. One of them is presented in Fig. 1c. By analyzing the data obtained, the periodicity in the density change along the specimen length can be perceived. Measurements showed that the period of density value oscillation lies within $(3.2\text{-}4.1)\cdot 10^{-3}$ limits. Such an interval of the oscillation period corresponds to the width of the braid that is formed while winding the shell.

As was noted above, investigation of specimen internal structure on a tomograph permitted construction and approximation of the function for the change in the mathematical expectation of the density over the specimen thickness. These data can be utilized to go over to estimation of the porosity of the composites under investigation. Let us recall that the data obtained refer to specimens cut out of a preloaded shell. Consequently, the porosity is predetermined in this case by the cracking of the binder during loading. Moreover, the specimens went through preliminary drying. We will characterize the porosity by the volume content of pores μ_p. The density of the polymer can be determined from the formula

$$\rho_{den} = \mu_f \rho_f + \mu_b \rho_b + \mu_p \rho_p. \quad (9)$$

Taking into account that $\mu_f + \mu_b + \mu_p = 1$, $\rho_p \approx 0$, it can be written in the form

$$\rho_{den} = \mu_f \rho_f + (1 - \mu_f - \mu_p)\rho_b. \quad (10)$$

We hence find μ_p:

$$\mu_p = \frac{\mu_f \rho_f + (1 - \mu_f)\rho_b - \rho_{den}}{\rho_b}. \quad (11)$$

The results of computations for one of the specimens under investigation by using (11) show that the maximal material porosity corresponds to a thickness with minimal density.

The density of a dry specimen determined by using a tomograph is $\rho_{den} = 1{,}110 \cdot 10^{-3}$ kg/m³. Let us assume that all the pores in the specimen are filled with water. Then after computations by using (8), we obtain $\rho_{den} = 1{,}314 \cdot 10^{-3}$ m. Under ordinary conditions, specimens are in the equilibrium state with the surrounding air, consequently

$$1{,}110 \cdot 10^{-3} \leqslant \rho_{den} \leqslant 1{,}314 \cdot 10^{-3} \text{ (kg/m}^3\text{)}.$$

The limits of variation in the density values will be different under other conditions for conducting the experiment.

NOTATION

I_o, intensity of incident radiation on the specimen surface; L, quantity of approximating points; n, degree of the polynomial; μ_f, volume content of bonding filler; μ_b, μ_p, volume contents of binder and pores; ρ_f, ρ_b, filler and binder densities, respectively; ρ_p, air density in the pores; and k, number of repetitions.

LITERATURE CITED

1. H. G. Scudder, TIIER, 66, No. 6, 5-16 (1978).
2. V. V. Klyuev, É. I. Vainberg, I. A. Kazak, and V. P. Kurozaev, Defektoskopiya, No. 3, 42-50 (1980).

BASE DATA FOR ANALYSIS OF WATER VAPOR RADIATION CHARACTERISTICS

S. P. Detkov and O. A. Bryukhovskikh

UDC 536.3

Arrays of parameters are recommended for a narrowband spectrum model which represents the base data for analyzing the absorptivity, emissivity, and their derivatives for water vapor characteristics.

INTRODUCTION

Computations of the emissivity and absorptivity of water vapor are based on Hottel observations in the complete spectrum. Spectral data in a semiempirical treatment have appeared comparatively recently. Formulas are proposed in [1, 2] for the absorption in spectrum bands by utilization of a broadband model and an exponential envelope. Another base in the handbook [3] and its sources is represented in the form of two parameter arrays for a narrowband Goode model in 25 cm^{-1} wide spectrum intervals. Discrepancies in the results of integrated and spectral data were noted in a number of papers, for instance, in [4] and then in [5], where an Edwards computation was selected as base as being simpler as compared with the utilization of the Goode model. In this paper, on the other hand, as in Leckner, preference is given to two parameter arrays of a narrow band model. This base is more detailed, reliable, and ob-

All-Union Scientific-Research and Structural Design Institute of Metallurgical Thermal Engineering, Nonferrous Metallurgy, and Refractories, Sverdlovsk.

Translated from Inzhenerno-Fizicheskii Zhurnal, Vol. 51, No. 6, pp. 1027-1030, December, 1986. Original article submitted October 16, 1985.